Available online at www.sciencedirect.com
SCIENCE DIRECT®
International Journal of Heat and Mass Transfer 47 (2004) 887–898
International Journal of HEAT and MASS TRANSFER
www.elsevier.com/locate/ijhmt

Transient temperature computation of spheres in three-dimensional random packings

W.W.M. Siu, S.H.-K. Lee *

Department of Mechanical Engineering, Hong Kong University of Science and Technology, Clear Water Bay, Kowloon, Hong Kong

Received 10 May 2003; received in revised form 29 August 2003

Abstract

In this work, the Discrete Conduction Model (DCM method) was developed. This proposed method is an intermediate approach between the porous medium and PDE methods, as it assumes each sphere to be an isothermal element, and constructs the energy conservation equation in terms of thermal resistances between these contacting spheres. As a result, the governing equations were reduced to a set of simultaneous ODE's in time. To demonstrate this method, a packing algorithm was utilized to generate 3-D random packed beds, and the results showed the DCM method to have an error of less than 0.9% while attaining a speedup of 10^5 in comparison with the PDE method. In addition, results for varying packing structures showed the porosity to be insufficient to uniquely characterize a packing structure, but instead presents correlations in terms of CN and γ.

1. Introduction

Heat transfer in a porous medium is an area rich in practical applications, and has for decades attracted numerous researchers. By and large, most of these pioneering studies were driven by large-scale applications such as geothermal heating, but more recently there has been a growing interest in porous systems with smaller length-scale requirements. Applications include rapid-rate sintering [1], catalytic packed-bed [2], solid fuel-cell [3], insulation coating [4], and Microsystems [5].

For rapid-rate sintering, experiments have found it to be 1000 times faster than normal sintering, and the amount of time required to reach the theoretical density can be reduced from days (normal sintering) to minutes or even seconds [1]. Thus, this is an application rich in commercial and research value. However, this phenomenon was found to be related to thermal diffusion driven by the local temperature gradients, and unfortunately, researchers found modeling of this type of sintering to be "extremely difficult" because "the temperature–time profile is known only approximately" [6]. Catalytic packed-bed is another example of an application requiring improved heat transfer models to capture smaller length scales. In general, a catalytic packed-bed is a porous structure whereby chemical reactions occur as the working fluid flows through. Since heat is generally generated, catalytic packed-beds are designed to minimize thermally induced instabilities [2]. However, researchers found the existing heat transfer tools to either "appreciably over-predicts the hot spot" or require empirically determined parameters for each and every system for which predictions are sought [7].

Thus, while there is an abundance of porous-medium heat transfer studies, most of the earlier ones [c.f. 8] tended to assume the porous medium to be a continuous, macroscopic system with effective thermal properties (hereafter referred to as the effective-medium or porous medium approximation), and as such are more suitable for large-scale systems such as geothermal. Consequently, there have been fewer studies that are applicable for emerging areas with smaller length-scale requirements. There is, of course, always the option of directly solving the partial differential equation for each particle in the packing and then coupling them through the boundary conditions, but this would consume an excessive amount of computational resource, as it would

* Corresponding author.
E-mail address: shklee@ust.hk (S.H.-K. Lee).

0017-9310/$ - see front matter © 2003 Elsevier Ltd. All rights reserved.
doi:10.1016/j.ijheatmasstransfer.2003.08.022

Nomenclature

A	area, m^2
CN	Mean Coordination Number
C_p	specific heat capacity, W s/K
k	thermal conductivity, W/m K
M	total number of spheres in system
N	number of neighbor spheres in contact (local coordination number)
Q	total heat transfer, W
R	thermal constriction resistance, K/W
T	temperature, K
V	volume, m^3
X,Y,Z	dimensions of sphere packing

Greek symbols

α	thermal diffusivity, m^2/s
β	angle between two contacts, rad
δT	correction of the sphere temperature, K
γ	ratio of contact radius to sphere radius, r_c/r_s
τ	time, s
τ_{kj}	time parameter, s

Subscripts

b	bulk
c	contact
l	local
s	sphere, or length scale with r_s

render solutions at a length scale far smaller than required.

Besides the effective-medium approximation, there are a large variety of alternative approaches. In general, these approaches have in common the characteristic of not directly dealing with each particle in the packing structure, and as such would inherently have difficulties to later accommodate system-level convective and/or radiative exchanges. Two such studies are presented here for illustrative purposes, although it should be clear that there is an abundance of other studies sharing similar limitations. In 1997, Sahimi and Tsotsis [9] presented one of the earlier alternative models for the studies of pure conduction in a porous medium. Instead of adapting the classical effective-medium approximation, Sahimi presented an analytical model that could account for large-scale spatial variations in a random porous medium through the usages of various Green's functions. While this model certainly was a step forward in terms of its ability to account for spatial non-uniformities, it nonetheless relied on the availability of distribution functions that require a significant effort to determine, even if it existed for a non-Voronoi-type packing structure. In addition, it is not clear how or whether this formulation could be extended to 3-D configurations, and how it could be extended to include convective and radiative exchange. Another alternative approach was proposed by Cheng et al. [10], in which the packing structure was again modeled as a Voronoi polyhedron, and the effective conductivity was computed for a 3-D packing structure through circuit-type analyses. Again, this method could only be applied for regular packings, and is of limited value for random packings, transient calculations, or convective/radiative exchange.

In principle, it is possible to model each particle in the packing as isothermal spheres and to formulate the subsequent energy equation in terms of the resistance network. Thus, this method, herein referred to as the Discrete Conduction Model (DCM), has the potential of being a viable solution for applications requiring greater spatial resolution than that provided by the classical porous medium approach. While this DCM method is readily extendable to account for convective and radiative exchange, the major obstacle is that in assuming each sphere to be isothermal, it creates an artifact that limits its applicability to transient calculations. Thus, for the DCM method to be applicable for transient calculations, a correction term needs to be included. In 1999, Siu and Lee [11] called this the capacitance effect, but were only able to correlate it for the very restrictive configuration of spheres in linear (180-degree) contacts, as it was intimately tied to the packing configuration. Thus, in order to utilize the DCM method for transient, 3-D calculation, more work was required to determine the capacitance effect from each spheres couple in a complex, 3-D packing structure.

This is the motivation for the present study. The objectives are to develop the DCM method for transient, 3-D calculations, and to utilize the model to investigate the effects of packing structures on the effective thermal conductivity. Specifically, the interest is to determine whether porosity is sufficient to uniquely describe the thermal characteristic of a packed bed, and furthermore to elucidate on the interplay between the microstructure of the packing (coordination number and contact radius), the overall porosity and their effect on the effective conductivity. This is of particular relevance as many existing studies have validated results utilizing porosity as the characteristic parameter. In this regard, besides

elucidating on the above-mentioned interplay, this study seeks to reconcile any such interplay with the vast body of results already established. To accomplish these objectives, the constitutive relation was re-developed in order to capture the capacitance artifact between spheres in complex arrangements. The resulting transient energy equation was then executed for 3-D regular and random packings.

2. Analysis

The DCM method can be summarized below in Eq. (1), where as discussed in the earlier study [11], the Correction Term in the constitutive relation given by Eq. (1c) accounts for the capacitance effect necessary to offset the artificial diffusion induced by the assumption of isothermal spheres. In order to extend Eq. (1) to three-dimensional random packed beds, two issues needed to be addressed. First, as Eq. (1) was derived for a contact angle, β, of 180-degrees (Fig. 1a), the effect of different contact angles (Fig. 1b), needed to be verified. Second, as the number of contacts on each sphere increases (Fig. 1c), so too the amount of thermal energy diffusing in or out of each sphere, and, thus, the Correction Term needed to be revised in order to account for the number of contacting spheres.

$$T_i = \frac{1}{V}\int T\,\mathrm{d}V \tag{1a}$$

$$\rho C_\mathrm{p} V \frac{\mathrm{d}T_j}{\mathrm{d}\tau} = \sum_{i=1}^{N} Q_{ij}, \quad j = 1, M \tag{1b}$$

$$Q_{ij} = \frac{T_i - T_j}{R_{ij}} + (\text{Correction Term of the diffusion}) \tag{1c}$$

To account for the two above-mentioned issues, an alternative form of Eq. (1c) was used, whereby the effect of the previous Correction Term was now achieved through corrections in the driving potential, $T_i - T_j$. That is, the effects of the instantaneous diffusion, the contact angles and the number of contacting spheres were all addressed by correcting this driving potential. This is given below by Eq. (2), where the correlation given in Eq. (2b) was obtained from an earlier study [12]. Thus, the key to the Correction Term came down to determining the appropriate expression for the temperature correction, δT.

$$Q_{ij} = \frac{T_i' - T_j'}{R_{ij}} = \frac{(T_i - \delta T_i) - (T_j - \delta T_j)}{R_{ij}} \tag{2a}$$

$$R_{ij} = \frac{0.57588}{kr_\mathrm{s}\gamma}\left(1 - \frac{1.0920x10^{-3}}{\gamma} + \frac{3.0187x10^{-5}}{\gamma^2} - \frac{1.202x10^{-7}}{\gamma^3}\right) \tag{2b}$$

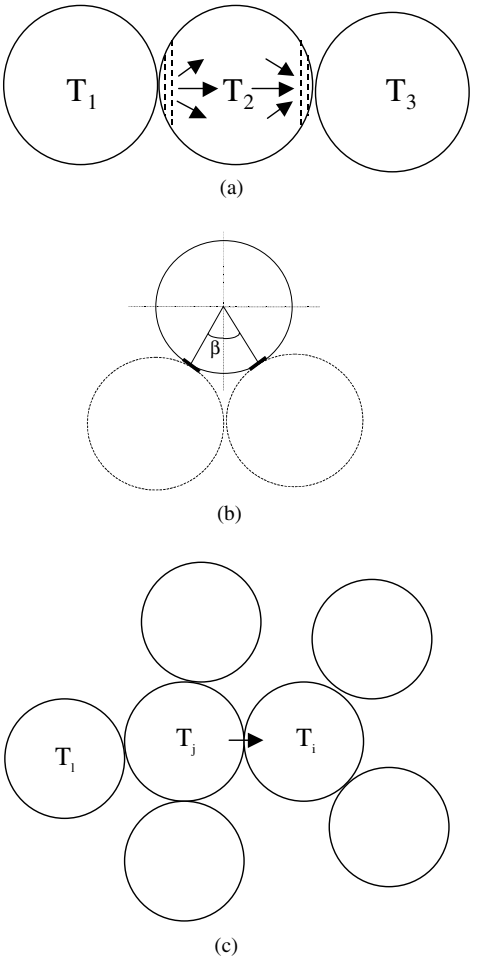

Fig. 1. Schematic of contacting sphere system with (a) 180 degree orientation (b) a varying contact angle, β and (c) multiple neighboring spheres.

2.1. Governing equation

To develop the expression for δT, the bulk temperature of sphere-j (Fig. 1c) can be conceptually thought of as consisting two components. One component is T_j', the average temperature of a small region in sphere-j that is in the immediate vicinity of the surface in contact with sphere-i; this is the temperature responsible for the heat flow across the contact. The second component, δT_j, is the temperature rise due to the thermal energy coming from other contacting spheres. Thus, the sum of these two components (T_j' and δT_j) gives the average temperature, T_j. Allowing Q_{lj} to represent the heat transfer from sphere-l to sphere-j, and assuming that it takes a duration of τ_{li} for this heat to propagate from sphere-l through sphere-j and arriving at sphere-i, then δT_j can be thought of as the additional "energy"

diffusing to sphere-i from sphere-j's neighboring spheres. Thus, assuming that including sphere-i, sphere-j has "N" additional neighboring spheres, then the expression for δT_j can be expressed by Eq. (3a). This δT_j is, thus, the component that needs to be subtracted from T_j in order to properly compute the energy exchange between sphere-j and sphere-i. Obviously the exact expression for δT_j depends on the choice of T_i, and it is thus a vector with N components if sphere-j has a total of N contacting spheres. This δT_j embodies a time constant, τ_{li}, which as given below in Eq. (3b) was found in an earlier study [13] to be proportional to half of the distance between sphere-l and sphere-i.

$$\delta T_j = \frac{1}{\rho C_p V}\sum_{\substack{l=1\\ l\neq i}}^{N}\left[\int_{\tau-\tau_{li}}^{\tau} Q_{lj}\,\mathrm{d}\tau\right] \tag{3a}$$

$$\tau_{li} = \frac{[r_s \sin(\beta_{li}/2)]^2}{\alpha} \tag{3b}$$

After invoking the trapezoidal rule, Eq. (3a) can be rewritten as Eq. (4a) below, and after invoking Taylor's expansion, truncating higher order terms, the expression for δT_j can be equivalently expressed by Eq. (4b).

$$\delta T_j = \frac{1}{\rho C_p V}\sum_{\substack{l=1\\ l\neq i}}^{N}\frac{1}{2}[Q_{lj}|_{\tau} + Q_{lj}|_{\tau-\tau_{li}}]\tau_{li} \tag{4a}$$

$$\delta T_j = \frac{1}{\rho C_p V}\sum_{\substack{l=1\\ l\neq i}}^{N}\left[Q_{lj} - \frac{1}{2}\frac{\mathrm{d}Q_{lj}}{\mathrm{d}\tau}\tau_{li} + \frac{1}{4}\frac{\mathrm{d}^2 Q_{lj}}{\mathrm{d}\tau^2}\tau_{li}^2\right]\tau_{li} \tag{4b}$$

Similarly, the same analyses can be performed for sphere-i, and thus, substituting these into Eq. (2a), the final governing equations take on the forms given below by Eq. (5).

$$Q_{ij} = \frac{T_i - T_j}{R_{ij}} - \frac{1}{R_{ij}\rho C_p V}\left\{\sum_{\substack{k=1\\ k\neq j}}^{N}\left[Q_{ki} - \frac{1}{2}\frac{\mathrm{d}Q_{ki}}{\mathrm{d}\tau}\tau_{kj} + \frac{1}{4}\frac{\mathrm{d}^2 Q_{ki}}{\mathrm{d}\tau^2}\tau_{kj}^2\right]\tau_{kj} - \sum_{\substack{l=1\\ l\neq i}}^{N}\left[Q_{lj} - \frac{1}{2}\frac{\mathrm{d}Q_{lj}}{\mathrm{d}\tau}\tau_{li} + \frac{1}{4}\frac{\mathrm{d}^2 Q_{lj}}{\mathrm{d}\tau^2}\tau_{li}^2\right]\tau_{li}\right\} \tag{5a}$$

$$\rho C_p V\frac{\mathrm{d}T_j}{\mathrm{d}\tau} = \sum_{i=1}^{N} Q_{ij}, \quad j = 1, M \tag{5b}$$

$$\tau_{li} = \frac{[r_s \sin(\beta_{li}/2)]^2}{\alpha} \tag{5c}$$

$$R_{ij} = \frac{0.57588}{k r_s \gamma}\left(1 - \frac{1.0920\times 10^{-3}}{\gamma} + \frac{3.0187\times 10^{-5}}{\gamma^2} - \frac{1.202\times 10^{-7}}{\gamma^3}\right) \tag{5d}$$

Note that since Eq. (5) was derived with a truncated Taylor's series, it is only valid for a time-scale, $\mathrm{d}\tau$, greater than the time constant, τ. For example, the time-scale, $\mathrm{d}\tau$, must be greater than 0.1 s for 1 mm glass beads and 1×10^{-3} s for 1 mm copper spheres.

2.2. Method of solution

Before solving Eq. (5), a packing structure first needs to be generated. This packing structure should contain information on the size and location of each sphere in the packed bed, as well as the contact radii formed between the contacting spheres within the packed bed. From this, basic information such as the contact-radius-to-sphere-radius ratio, γ, the contact angles between neighboring spheres, β, the time constants, τ, and the relevant constriction resistances, R, can all be determined. In the present study, we had utilized the packing algorithm developed in an earlier study [14] in order to obtain a three-dimensional-random packed-bed. Unless otherwise specified, 2 mm diameter stainless steel (AISI 304) spheres were used. The thermal conductivity, density, and specific heat capacity were 13.4, 468, and 8238, respectively, and contacts between the spheres were assumed to be perfect.

To illustrate the application of Eq. (5), a 4×4 2-D regular packing structure (Fig. 2) is utilized, although the results presented in this manuscript were obtained for random, 3-D packings. The first step in solving Eq. (5) is to setup Eq. (5a) for each of the 16 spheres in this example structure, in which these spheres are sorted as corner, boundary and internal spheres. Each of the four Corner spheres has two neighbors, and for sphere-1 in Fig. 2, they are sphere-2 and sphere-5. Looking strictly at the interaction between sphere-2 and sphere-1, the resulting heatflow is Q_{21}, and for this interaction, corrections are needed due to heat flowing into sphere-2 and sphere-1. Specifically, sphere-2 receives heat directly

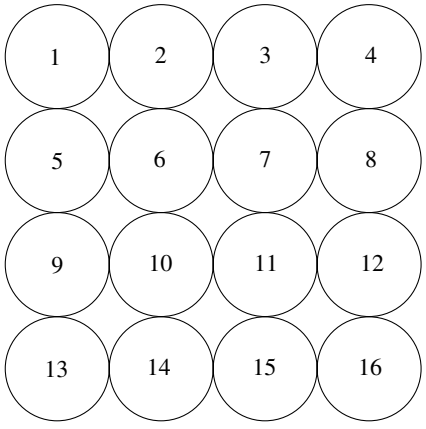

Fig. 2. Schematic of a 2-D packing utilized for illustrating the solution procedure.

from sphere-3 and sphere-6 while sphere-1 receives heat directly from sphere-5. Taking these into account, Eq. (5a) for Q_{21} is given below in Eq. (5a1).

$$\begin{aligned}Q_{21} &= \frac{T_2 - T_1}{R_{21}} \\ &\quad - \frac{1}{R_{21}\rho C_p V}\left\{\left[Q_{32} - \frac{1}{2}\frac{dQ_{32}}{d\tau}\tau_{31} + \frac{1}{4}\frac{d^2Q_{32}}{d\tau^2}\tau_{31}^2\right]\tau_{31}\right. \\ &\quad + \left[Q_{62} - \frac{1}{2}\frac{dQ_{62}}{d\tau}\tau_{61} + \frac{1}{4}\frac{d^2Q_{62}}{d\tau^2}\tau_{61}^2\right]\tau_{61} \\ &\quad \left. - \left[Q_{51} - \frac{1}{2}\frac{dQ_{51}}{d\tau}\tau_{52} + \frac{1}{4}\frac{d^2Q_{51}}{d\tau^2}\tau_{52}^2\right]\tau_{52}\right\} \qquad (5a1)\end{aligned}$$

A similar expression can similarly by focusing on, Q_{51}, the interaction between sphere-5 and sphere-1, and this is given below by Eq. (5a2).

$$\begin{aligned}Q_{51} &= \frac{T_5 - T_1}{R_{51}} \\ &\quad - \frac{1}{R_{51}\rho C_p V}\left\{\left[Q_{65} - \frac{1}{2}\frac{dQ_{65}}{d\tau}\tau_{61} + \frac{1}{4}\frac{d^2Q_{65}}{d\tau^2}\tau_{61}^2\right]\tau_{61}\right. \\ &\quad + \left[Q_{95} - \frac{1}{2}\frac{dQ_{95}}{d\tau}\tau_{91} + \frac{1}{4}\frac{d^2Q_{95}}{d\tau^2}\tau_{91}^2\right]\tau_{91} \\ &\quad \left. - \left[Q_{21} - \frac{1}{2}\frac{dQ_{21}}{d\tau}\tau_{25} + \frac{1}{4}\frac{d^2Q_{21}}{d\tau^2}\tau_{25}^2\right]\tau_{25}\right\} \qquad (5a2)\end{aligned}$$

Thus, two equations are generated for each corner sphere, with each corresponding to an interaction pair, and the relevant expressions for the time constants, τ, and resistance, R are obtained through Eqs. (5c) and (5d). Besides corner spheres, the packing in Fig. 2 also contains eight boundary spheres, with each being in contact with three neighboring spheres. As a result, there is three interacting pairs for each boundary sphere, and from the discussions above, there is a governing equation for each of the interacting pairs. That is, for each boundary sphere in this 2-D example, there are three equations. Consider for example, sphere-5 in Fig. 2, which is in contact with sphere-1, sphere-6 and sphere-9, and consequently giving rise to Q_{15}, Q_{65}, and Q_{95}. For Q_{15}, the energy for sphere-1 needs to account for the energy coming from sphere-2, while for sphere-5, corrections are needed due to energy coming from sphere-6 and sphere-9. Similar considerations are given for each of the other two interacting pairs, and the resulting equation is given below in Eq. (5a3)

$$\begin{aligned}Q_{15} &= \frac{T_1 - T_5}{R_{15}} \\ &\quad - \frac{1}{R_{15}\rho C_p V}\left\{\left[Q_{21} - \frac{1}{2}\frac{dQ_{21}}{d\tau}\tau_{25} + \frac{1}{4}\frac{d^2Q_{21}}{d\tau^2}\tau_{25}^2\right]\tau_{25}\right. \\ &\quad - \left[Q_{65} - \frac{1}{2}\frac{dQ_{65}}{d\tau}\tau_{61} + \frac{1}{4}\frac{d^2Q_{65}}{d\tau^2}\tau_{61}^2\right]\tau_{61} \\ &\quad \left. - \left[Q_{95} - \frac{1}{2}\frac{dQ_{95}}{d\tau}\tau_{91} + \frac{1}{4}\frac{d^2Q_{95}}{d\tau^2}\tau_{91}^2\right]\tau_{91}\right\}\end{aligned}$$

$$\begin{aligned}Q_{65} &= \frac{T_6 - T_5}{R_{65}} \\ &\quad - \frac{1}{R_{65}\rho C_p V}\left\{\left[Q_{26} - \frac{1}{2}\frac{dQ_{26}}{d\tau}\tau_{25} + \frac{1}{4}\frac{d^2Q_{26}}{d\tau^2}\tau_{25}^2\right]\tau_{25}\right. \\ &\quad + \left[Q_{76} - \frac{1}{2}\frac{dQ_{76}}{d\tau}\tau_{75} + \frac{1}{4}\frac{d^2Q_{76}}{d\tau^2}\tau_{75}^2\right]\tau_{75} \\ &\quad + \left[Q_{10-6} - \frac{1}{2}\frac{dQ_{10-6}}{d\tau}\tau_{10-5} + \frac{1}{4}\frac{d^2Q_{10-6}}{d\tau^2}\tau_{10-5}^2\right]\tau_{10-5} \\ &\quad - \left[Q_{15} - \frac{1}{2}\frac{dQ_{15}}{d\tau}\tau_{16} + \frac{1}{4}\frac{d^2Q_{15}}{d\tau^2}\tau_{16}^2\right]\tau_{16} \\ &\quad \left. - \left[Q_{95} - \frac{1}{2}\frac{dQ_{95}}{d\tau}\tau_{96} + \frac{1}{4}\frac{d^2Q_{95}}{d\tau^2}\tau_{96}^2\right]\tau_{96}\right\}\end{aligned}$$

$$\begin{aligned}Q_{95} &= \frac{T_9 - T_5}{R_{95}} - \frac{1}{R_{95}\rho C_p V} \\ &\quad \times \left\{\left[Q_{10-9} - \frac{1}{2}\frac{dQ_{10-9}}{d\tau}\tau_{10-5} + \frac{1}{4}\frac{d^2Q_{10-9}}{d\tau^2}\tau_{10-5}^2\right]\tau_{10-5}\right. \\ &\quad + \left[Q_{13-9} - \frac{1}{2}\frac{dQ_{13-9}}{d\tau}\tau_{13-5} + \frac{1}{4}\frac{d^2Q_{13-9}}{d\tau^2}\tau_{13-5}^2\right]\tau_{13-5} \\ &\quad - \left[Q_{15} - \frac{1}{2}\frac{dQ_{15}}{d\tau}\tau_{19} + \frac{1}{4}\frac{d^2Q_{15}}{d\tau^2}\tau_{19}^2\right]\tau_{19} \\ &\quad \left. - \left[Q_{65} - \frac{1}{2}\frac{dQ_{65}}{d\tau}\tau_{69} + \frac{1}{4}\frac{d^2Q_{65}}{d\tau^2}\tau_{69}^2\right]\tau_{69}\right\} \qquad (5a3)\end{aligned}$$

Having completed the derivation for the corner and boundary spheres, it requires only a simple extension of the same principle to obtain the governing equations for the interior spheres. For sphere-6 in Fig. 2, it is in contact with four neighboring spheres, and, thus, a total of four equations are generated with each corresponding to each of the four interactions: Q_{26}, Q_{56}, Q_{76}, and Q_{10-6}. These equations are given below in Eq. (5a4).

$$\begin{aligned}Q_{26} &= \frac{T_2 - T_6}{R_{26}} \\ &\quad - \frac{1}{R_{26}\rho C_p V}\left\{\left[Q_{12} - \frac{1}{2}\frac{dQ_{12}}{d\tau}\tau_{16} + \frac{1}{4}\frac{d^2Q_{12}}{d\tau^2}\tau_{16}^2\right]\tau_{16}\right. \\ &\quad + \left[Q_{32} - \frac{1}{2}\frac{dQ_{32}}{d\tau}\tau_{36} + \frac{1}{4}\frac{d^2Q_{32}}{d\tau^2}\tau_{36}^2\right]\tau_{36} \\ &\quad - \left[Q_{56} - \frac{1}{2}\frac{dQ_{56}}{d\tau}\tau_{52} + \frac{1}{4}\frac{d^2Q_{56}}{d\tau^2}\tau_{52}^2\right]\tau_{52} \\ &\quad - \left[Q_{76} - \frac{1}{2}\frac{dQ_{76}}{d\tau}\tau_{72} + \frac{1}{4}\frac{d^2Q_{76}}{d\tau^2}\tau_{72}^2\right]\tau_{72} \\ &\quad \left. - \left[Q_{10-6} - \frac{1}{2}\frac{dQ_{10-6}}{d\tau}\tau_{10-2} + \frac{1}{4}\frac{d^2Q_{10-6}}{d\tau^2}\tau_{10-2}^2\right]\tau_{10-2}\right\}\end{aligned}$$

$$
\begin{aligned}
Q_{56} = {} & \frac{T_5 - T_6}{R_{56}} \\
& - \frac{1}{R_{56}\rho C_p V}\left\{\left[Q_{15} - \frac{1}{2}\frac{dQ_{15}}{d\tau}\tau_{16} + \frac{1}{4}\frac{d^2Q_{15}}{d\tau^2}\tau_{16}^2\right]\tau_{16}\right. \\
& + \left[Q_{95} - \frac{1}{2}\frac{dQ_{95}}{d\tau}\tau_{96} + \frac{1}{4}\frac{d^2Q_{95}}{d\tau^2}\tau_{96}^2\right]\tau_{96} \\
& - \left[Q_{26} - \frac{1}{2}\frac{dQ_{26}}{d\tau}\tau_{25} + \frac{1}{4}\frac{d^2Q_{26}}{d\tau^2}\tau_{25}^2\right]\tau_{25} \\
& - \left[Q_{76} - \frac{1}{2}\frac{dQ_{76}}{d\tau}\tau_{75} + \frac{1}{4}\frac{d^2Q_{76}}{d\tau^2}\tau_{75}^2\right]\tau_{75} \\
& \left. - \left[Q_{10-6} - \frac{1}{2}\frac{dQ_{10-6}}{d\tau}\tau_{10-5} + \frac{1}{4}\frac{d^2Q_{10-6}}{d\tau^2}\tau_{10-5}^2\right]\tau_{10-5}\right\}
\end{aligned}
$$

$$
\begin{aligned}
Q_{76} = {} & \frac{T_7 - T_6}{R_{76}} - \frac{1}{R_{76}\rho C_p V} \\
& \times \left\{\left[Q_{37} - \frac{1}{2}\frac{dQ_{37}}{d\tau}\tau_{36} + \frac{1}{4}\frac{d^2Q_{37}}{d\tau^2}\tau_{36}^2\right]\tau_{36}\right. \\
& + \left[Q_{87} - \frac{1}{2}\frac{dQ_{87}}{d\tau}\tau_{86} + \frac{1}{4}\frac{d^2Q_{87}}{d\tau^2}\tau_{86}^2\right]\tau_{86} \\
& + \left[Q_{11-7} - \frac{1}{2}\frac{dQ_{11-7}}{d\tau}\tau_{11-6} + \frac{1}{4}\frac{d^2Q_{11-7}}{d\tau^2}\tau_{11-6}^2\right]\tau_{11-6} \\
& - \left[Q_{26} - \frac{1}{2}\frac{dQ_{26}}{d\tau}\tau_{27} + \frac{1}{4}\frac{d^2Q_{26}}{d\tau^2}\tau_{27}^2\right]\tau_{27} \\
& - \left[Q_{56} - \frac{1}{2}\frac{dQ_{56}}{d\tau}\tau_{57} + \frac{1}{4}\frac{d^2Q_{56}}{d\tau^2}\tau_{57}^2\right]\tau_{57} \\
& \left. - \left[Q_{10-6} - \frac{1}{2}\frac{dQ_{10-6}}{d\tau}\tau_{10-7} + \frac{1}{4}\frac{d^2Q_{10-6}}{d\tau^2}\tau_{10-7}^2\right]\tau_{10-7}\right\}
\end{aligned}
$$

$$
\begin{aligned}
Q_{10-6} = {} & \frac{T_{10} - T_6}{R_{10-6}} - \frac{1}{R_{10-6}\rho C_p V} \\
& \times \left\{\left[Q_{9-10} - \frac{1}{2}\frac{dQ_{9-10}}{d\tau}\tau_{96} + \frac{1}{4}\frac{d^2Q_{9-10}}{d\tau^2}\tau_{96}^2\right]\tau_{96}\right. \\
& + \left[Q_{11-10} - \frac{1}{2}\frac{dQ_{11-10}}{d\tau}\tau_{11-6} + \frac{1}{4}\frac{d^2Q_{11-10}}{d\tau^2}\tau_{11-6}^2\right]\tau_{11-6} \\
& + \left[Q_{14-10} - \frac{1}{2}\frac{dQ_{14-10}}{d\tau}\tau_{14-6} + \frac{1}{4}\frac{d^2Q_{14-10}}{d\tau^2}\tau_{14-6}^2\right]\tau_{14-6} \\
& - \left[Q_{26} - \frac{1}{2}\frac{dQ_{26}}{d\tau}\tau_{2-10} + \frac{1}{4}\frac{d^2Q_{26}}{d\tau^2}\tau_{2-10}^2\right]\tau_{2-10} \\
& - \left[Q_{56} - \frac{1}{2}\frac{dQ_{56}}{d\tau}\tau_{5-10} + \frac{1}{4}\frac{d^2Q_{56}}{d\tau^2}\tau_{5-10}^2\right]\tau_{5-10} \\
& \left. - \left[Q_{76} - \frac{1}{2}\frac{dQ_{76}}{d\tau}\tau_{7-10} + \frac{1}{4}\frac{d^2Q_{76}}{d\tau^2}\tau_{7-10}^2\right]\tau_{7-10}\right\}
\end{aligned}
\tag{5a4}
$$

Assuming an initial temperature distribution, Eq. (5a) became an ODE in terms of Q_{ij}'s for all i's and j's, and for a packing of M spheres where each sphere has N contacting neighbors, this would yield a total of $M \times N$ ODE's for Q_{ij}'s. To solve Eq. (5a), the temperature from a previous time-step (or from initial condition) was utilized, and the derivatives were approximated using a backward-differencing scheme (fully implicit). Each of the resulting $M \times N$ algebraic equation was then successively solved once. The Q_{ij}'s were then placed into Eq. (5b), where the derivative term was also approximated using a backward-differencing scheme. The updated temperature distribution was then placed back into Eq. (5a) and the process iterated at the same time-step until the temperature reached the convergence criterion of 10^{-13}. Once iterative convergence was achieved within one time-step, the calculation proceeded to the next time-step and the entire process was repeated until steady-state was reached according to the infinity norm condition.

3. Results and discussion

After the typical verifications (user prescribed parameters and physical consistency), the numerical model was validated and results were obtained to assess the performance of the present model and the effects of various packing structures. The validation was structured to compare solutions at two different levels. The first-level validation consisted of comparing the sphere-temperature for a simple packing structure, while the second-level consisted of comparing the effective thermal conductivity for complex three-dimensional random packing structures. For the first-level validation, the results obtained from the presently proposed method were benchmarked against results obtained by solving the full partial differential equation (PDE method). For the second-level validation, the effective conductivity was computed from the temperature distribution obtained from the presently proposed method, and this was in-turn bench-marked against experimental results from the literature.

3.1. Validation

Shown in Fig. 3a is a system consisting of three contacting spheres, with sphere-1 initially at 10 °C while sphere-2 and sphere-3 were at 2.5 °C. At time $\tau = 0$, the three spheres were brought into contact with a contact angle, γ, of 140°, and as shown in Fig. 2b, nearly exact agreement was obtained between the solution obtained from the presently proposed DCM method and the volumetrically averaged solution obtained from the PDE method (each sphere was gridded with $20 \times 30 \times 30$ grids).

For systems containing more than three spheres, the PDE method required an excessive amount of computational time, and as a result, comparisons for such systems were made against existing experimental data on thermal conductivities. Shown in Fig. 4, is a schematic

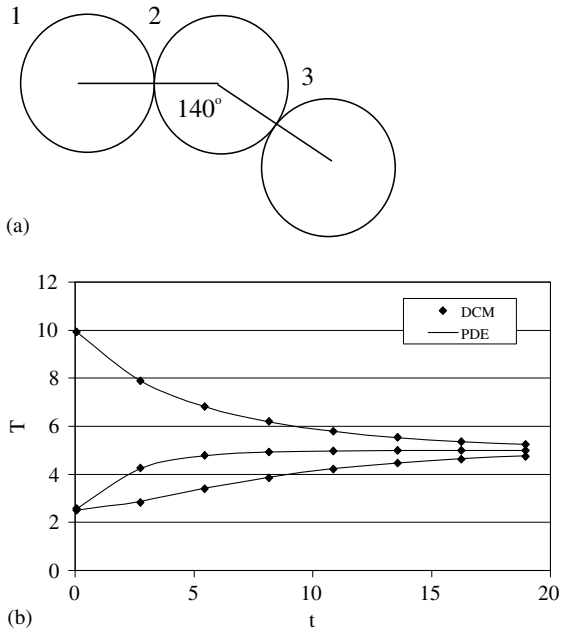

Fig. 3. Schematic of (a) the configuration used for the validation comparison against the PDE method and (b) comparison of the results obtained by the DCM and PDE methods.

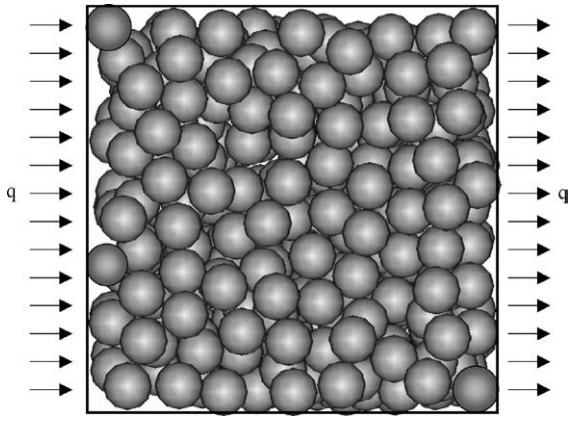

Fig. 4. Schematic of a typical three-dimensional random-packing structure used in the present study.

of typical three-dimensional random packings utilized in this study. Altogether, a packing of porosity 0.44 (500 spheres of 2 mm diameter) and a second packing of porosity 0.6 (503 sphere of 2 mm diameter) were studied. A heat-input boundary condition was imposed on one side and a heat-withdrawal boundary condition was imposed on the opposite side. Using the DCM method, the transient temperature of each sphere was computed until steady-state, and from this, the average planar temperatures and effective conductivity were calculated.

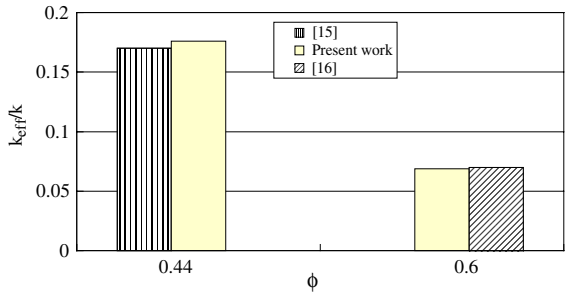

Fig. 5. Comparisons at different porosity of the effective thermal conductivity obtained by the DCM method and from existing experimental measurements.

Shown in Fig. 5, the results obtained from the DCM method was within 3% of measurements made by Koh et al. [15] and Agapiou and DeVires [16]. Besides direct comparisons, validation was also inferred for situations in which directly comparable solutions were not available. Shown in Fig. 6a is a schematic of a 3-D, regular packed bed consisting of five layers of spheres, where each layer consisted of nine spheres in contact. A unidirectional heat-flux was imposed and the resulting transient temperature was compared against results obtained from five spheres in linear contact (Fig. 6b). As expected, due to the symmetry in the problem, Fig. 6c and d show that the results obtained from the 45-sphere system agree with those obtained from the simplified 5-sphere system. That is, in the sense that the transient calculations in 2-D contacts were validated through Fig. 3, the validation for transient calculations in 3-D packings can be inferred from Fig. 6c. Finally, to confirm the necessity of the correction terms in Eq. (1c), comparisons were made with transient calculations on a 3-D packing structure subjected to 3-D heat-flux (Fig. 7a). The results in Fig. 7b showed the neglect of the correction term to introduce an error of roughly 10%, which can be considerable for applications such as rapid rate sintering.

3.2. Accuracy and computational efficiency

The simple and random packings used in the validation were employed to assess the accuracy and speedup of the DCM relative to the PDE and porous medium method. For the three-sphere case considered in Fig. 3, the DCM method was shown in Fig. 8 to be accurate to better than 0.9% when compared against solutions from the PDE method. As expected, the maximum error occurred at the boundary where the thermal gradient was largest. However, this minor error came at the benefit of a significant speed-up. As shown in Table 1, the DCM method required 0.5 CPU-second on a DEC-alpha 21164-500au workstation, while the

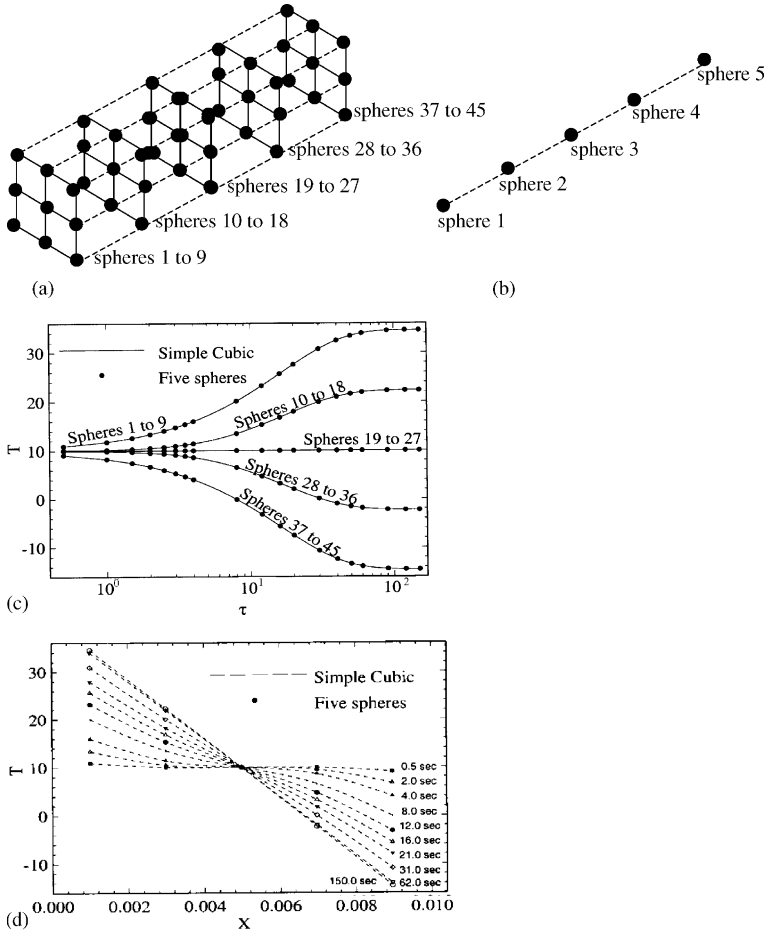

Fig. 6. Schematic of (a) a five-layer simple-cubic packing structure, (b) five spheres in linear contacts, (c) the transient temperature distribution from these two packing structures and (d) the planar temperature distributions.

PDE method required 15 CPU-hours even while using the more efficient Multi-Spatial-Temporal-Grid method [17]. This corresponded to a speedup of 10^5.

For a larger random packing of 503 spheres (porosity of 0.6), a similar comparison was made between the DCM and the porous medium method. Shown in Fig. 9a are the results obtained from these two methods, where due to the volumetric averaging the results from the porous medium method was shown in Fig. 9b to be off by as much as 80% on a local temperature basis. To demonstrate that this error stemmed from the volumetric averaging of the porous medium method, this comparison was repeated in Fig. 10a where the DCM solutions were averaged on a plane. In this case, the error from the porous medium method was shown in Fig. 10b to reduce from 80% to 10%. However, as summarized in Table 2, the low accuracy of the porous medium method comes with a speedup of 480 in comparison with the DCM method. Thus, for calculations not requiring spatial resolutions, the porous medium method can be an attractive choice.

3.3. Effect of packing structure

To illustrate the isotropy of a 3-D random packed bed, calculations were performed on a packed bed of 504 spheres with a mean coordination number, CN, and contact radius ratio, γ, of 3.7 and 3%, respectively. Shown in Fig. 11a, b and c are the temperature distributions resulting from unidirectional heat-flux conditions in the x, y and z directions, respectively. From the temperature distributions, the effective conductivities in the three directions were calculated and found in Fig. 12 to have a high degree of isotropy. This confirms the random nature of the packing structure.

One of the stated objectives of this study is to determine the parameters necessary to uniquely characterize the packed bed. To accomplish this, a large

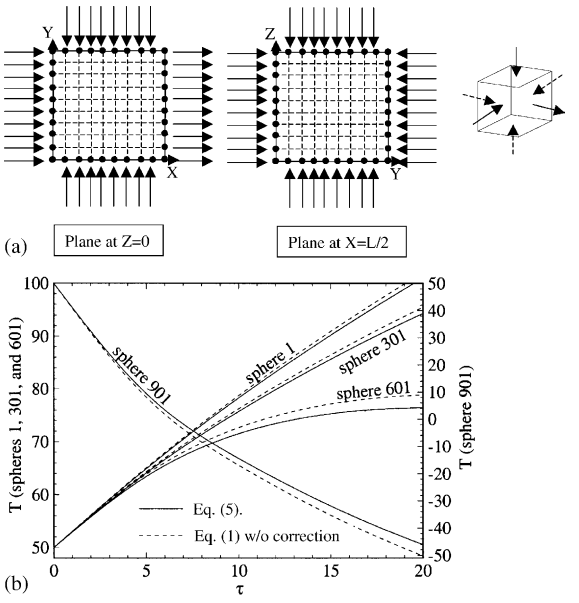

Fig. 7. Schematic showing (a) the heat-flux condition on a 3-D packing system and (b) the error induced in neglecting the correction term.

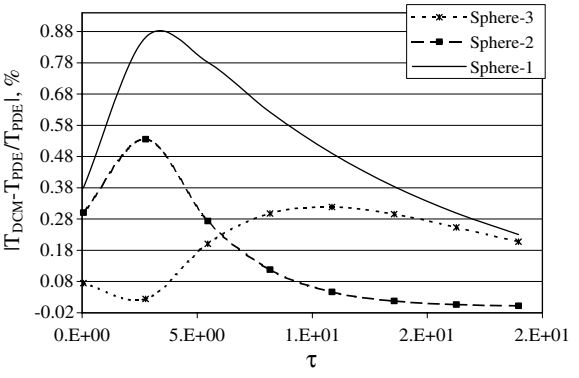

Fig. 8. Schematic showing the error between the DCM and PDE methods for different spheres in the packing and at different time.

Table 1
Performance comparison between DCM and PDE methods

	DCM method	PDE method
Computational time	0.5 CPU-second	15 CPU-hours
Speedup of DCM	10^5	
Error from DCM	Less than 0.9%	

number of random packings were generated over a range CN and γ, and the resulting effective conductivities were compared. As porosity is typically used to characterize packed beds, the results were plotted against porosities, but as shown in Fig. 13, packed beds with very similar porosity were found to have significantly different thermal conductivities. This clearly indicate that porosity is not sufficient to uniquely describe the packed bed, and further investigations revealed that packings with different microstructures can give rise to the same porosity. This is shown in Fig. 14a where the porosity was found to be a function of CN and r_c (through $\gamma = r_c/r_s$), but the effect of the microstructure was found to be greater at lower porosity and to decrease with increasing porosity. This is consistent with the larger scattering found at a porosity of 0.2 in Fig. 13. With these findings, the thermal conductivities shown in Fig. 13 were re-plotted against CN and γ, and as shown in Fig. 14b, the scatter in the data disappeared. Further effort to correlate the data resulted in the correlation given below in Eq. (6), which as shown in Fig. 15 attained a correlation coefficient of 0.9.

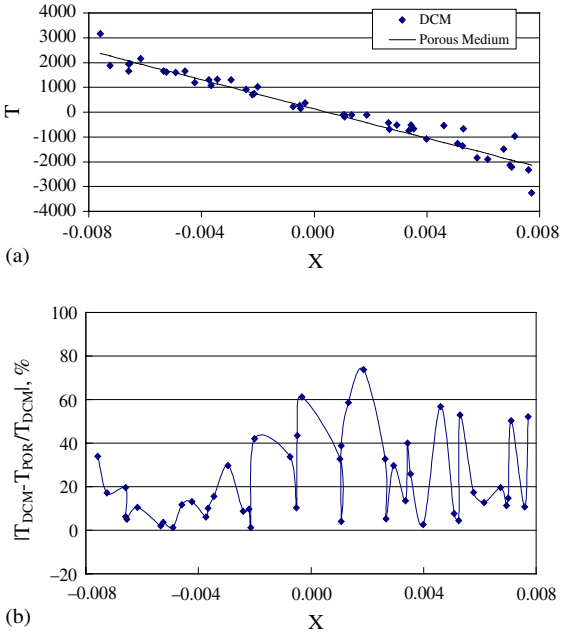

Fig. 9. Comparison between the results from the DCM and porous medium methods in terms of (a) the temperature distribution and (b) the percentage differences.

$$\frac{k_{\text{eff}}}{k_\gamma} = 0.0125\text{CN}^2 + 0.0716\text{CN} \tag{6}$$

Having shown that the thermal conductivity of a packed bed is a function of the packing structure, we now need to reconcile this with previous findings that found porosity to be sufficient in characterizing a packed bed. It turns out that many of the previous studies were performed on sintered packed beds, and in such case the

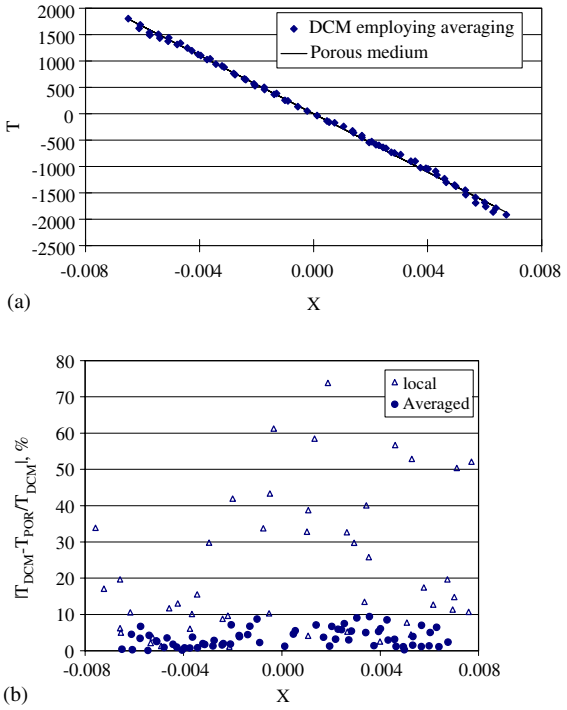

Fig. 10. Schematic showing the agreement between the porous medium results and planar-averaged DCM results in terms of (a) the temperature distribution and (b) the percentage differences.

Table 2
Performance comparison between DCM and porous medium methods

	DCM method	Porous medium method
Computational time	8 CPU-minutes	1 CPU-second
Speedup of porous medium method	480	
Error of porous medium method	80%	

two parameters (CN and γ) become non-independent [18]. In other words, while the porosity of packed bed is, in general, dependent on two independent, microstructural parameters (CN and γ), certain processes will remove the independence of these two parameters, and thus render a unique relation between the porosity and the packing microstructure. To verify this, the data in Fig. 13 were screened according to the microstructural relation for sintered packed beds [18], and the subsequent results in Fig. 16 showed considerable agreement with results found in the literature [15,16,19,20]. To

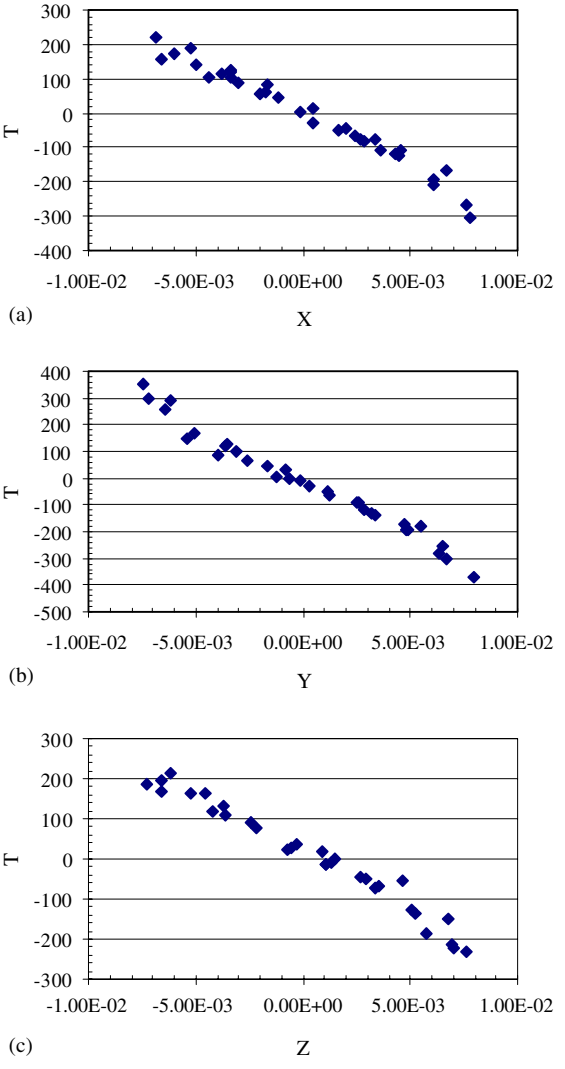

Fig. 11. Temperature distribution resulting from unidirectional heat-flux conditions in (a) x direction, (b) y direction and (c) z direction.

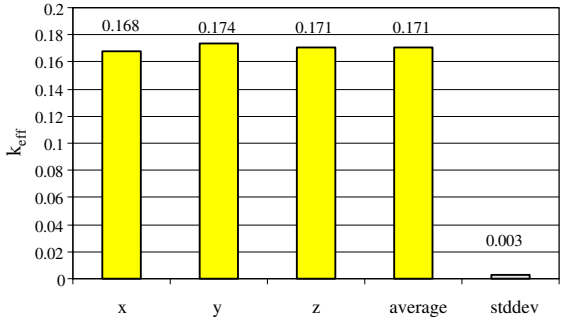

Fig. 12. Schematic showing the isotropy in the effective thermal conductivity of a 3-D random packed bed.

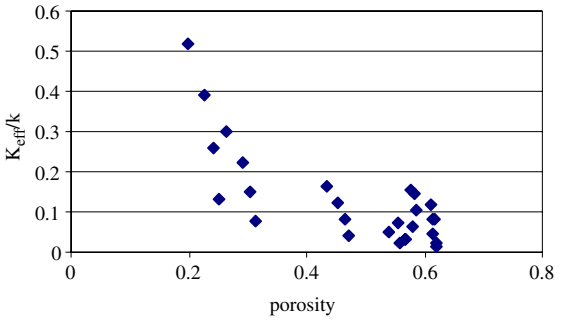

Fig. 13. Plot showing packing structures with the same porosity but different effective thermal conductivities.

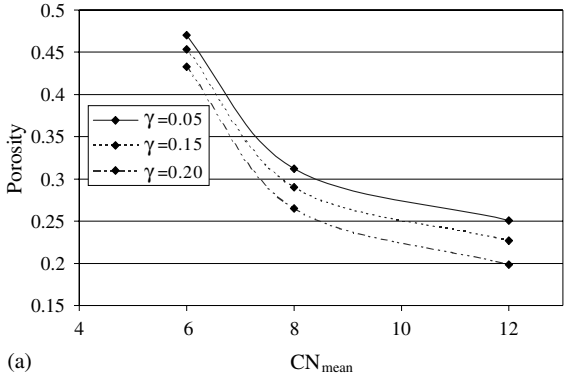

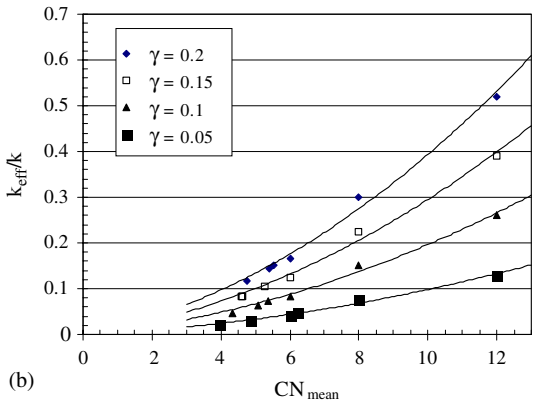

Fig. 14. Plot of the (a) porosity and (b) dimensionless effective conductivity against the microstructure of the random packed bed (mean CN number and mean contact radius ratio).

enable easier comparison, the presently computed results were also presented through a correlation assuming a third order polynomial dependence, which is given below in Eq. (7).

$$\frac{k_{\text{eff}}}{k} = -0.9\phi^3 + 2.8\phi^2 - 2.9\phi + 1 \qquad (7)$$

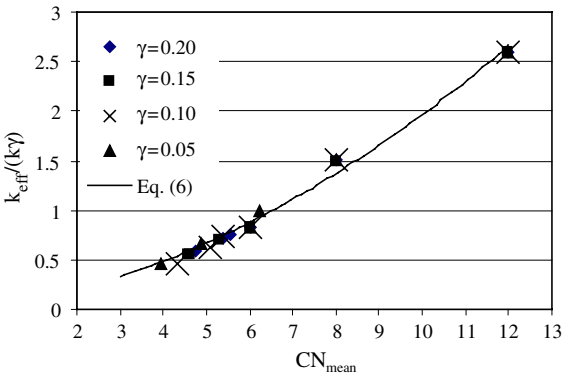

Fig. 15. Plot showing the correlation of the normalized effective conductivity against the microstructural parameters of the packings.

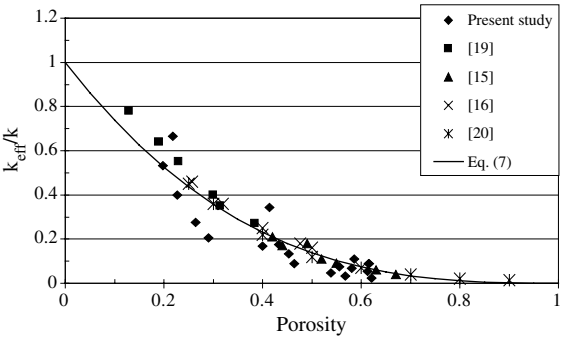

Fig. 16. Comparison of the screened results against the experimental result from the literature.

4. Conclusion

A DCM method was developed to enable 3-D transient calculations in random packed beds. To accomplish this, correction terms were developed to account for the relation between the capacitance effect and the packing structure. The resulting model was validated and then benchmarked for performance and accuracy. The results showed the current DCM method to be accurate to within 0.9% of solutions obtained by the PDE method, but at a speedup of 10^5. The results also showed the porosity to be insufficient to uniquely characterize a packing structure, but the parameters should instead be CN and γ. Correlations were presented relating the effective thermal conductivity to CN and γ.

Acknowledgements

The authors would like to acknowledge the financial support from the Department of Mechanical Engineering

at HKUST, and the Research Grant Council of Hong Kong (Grant #HKUST6237/00E, #HKUST6192/03E).

References

[1] R.M. Young, R. McPherson, Temperature-gradient-driven diffusion in rapid-rate sintering, Journal of the American Ceramic Society 72 (6) (1988) 1080–1081.
[2] V. Balakotaiah, E.L. Christoforatou, D.H. West, Transverse concentration and temperature nonuniformities in adiabatic packed-bed catalytic reactors, Chemical Engineering Science 54 (1999) 1725–1734.
[3] S. De Souza, S.J. Visco, L.C. DeJonghe, Reduced-temperature solid oxide fuel cell based on YSZ thin-film electrolyte, Journal of the Electrochemical Society 144 (3) (1997) L35–L37.
[4] K.W. Schlichting, N.P. Padture, P.G. Klemens, Thermal conductivity of dense and porous yttria-stabilized zirconia, Journal of Materials Science 36 (2001) 3003–3010.
[5] S. Périchon, V. Lysenko, Ph. Roussel, B. Remaki, B. Champagnon, D. Barbier, P. Pinard, Technology and micro-Raman characterization of thick meso-porous silicon layers for thermal effect microsystems, Sensors and Actuators 85 (2000) 335–339.
[6] D.L. Johnson, Comment on temperature-gradient-driven diffusion in rapid-rate sintering, Journal of the American Ceramic Society 73 (8) (1990) 2576–2578.
[7] K. Kamiuto, S. Saitoh, Simultaneous heat and mass transfer in packed bed catalytic reactors, Journal of Thermophysics and Heat Transfer 9 (3) (1995) 524–530.
[8] C.L. Tien, Thermal radiation in packed and fluidized beds, Journal of Heat Transfer 110 (1988) 1230–1242.
[9] M. Sahimi, T.T. Tsotsis, Transient diffusion and conduction in heterogeneous media: beyond the classical effective medium approximation, Industrial Engineering and Chemical Research 36 (1997) 3043–3052.
[10] G.J. Cheng, A.B. Yu, P. Zulli, Evaluation of effective thermal conductivity from the structure of a packed bed, Chemical Engineering Science 54 (1999) 4199–4209.
[11] W.W.M. Siu, S.H.-K. Lee, Transient temperature computation for a system of multiply contacting spheres in 180-degree orientation, Journal of Heat Transfer 121 (1999) 739–742.
[12] W.W.M. Siu, S.H.-K. Lee, Transient effect on the constriction resistance between spheres, Computational Mechanics 25 (2000) 59–65.
[13] W.W.M. Siu, S.H.-K. Lee, The effect of Geometrical Arrangement on the Transient Temperature Computation of Contacting Spheres, In: Proceeding of ASME International Mechanical Engineering Congress and Exposition, vol. 361-1, Anaheim, CA, USA, ASME Publication HTD-, 1998, pp. 285–297.
[14] A.K.C. Wu, S.H.-K. Lee, Sphere packing algorithm for heat transfer studies, Numerical Heat Transfer—Part A 37 (6) (2000) 631–652.
[15] J.C.Y. Koh, E.P. Casal, R.W. del Evans, V. Derlugin, Fluid flow and heat transfer in high temperature porous matrices for transpiration cooling, AFFDL-TR-66-70, 1966.
[16] J.S. Agapiou, M.F. DeVries, An experimental determination of the thermal conductivity of a 304L stainless steel powder metallurgy material, Journal of Heat Transfer 111 (1989) 281–286.
[17] W.W.M. Siu, S.H.-K. Lee, Multi-spatial-temporal grids for three-dimensional transient conduction problems, Numerical Heat Transfer—Part B 26 (1999) 163–181.
[18] E. Arzt, The influence of an increasing particle coordination in the densification of spherical powders, Acta Metallurgy 30 (1982) 1833–1890.
[19] J.C.Y. Koh, A. Fortini, Thermal Conductivity and Electrical Resistivity of Porous Material, NASA report CR-120854, 1971.
[20] S. Torquato, I.C. Kim, D. Cule, Effective conductivity, dielectric constant, and diffusion coefficient of digitized composite media via first-passage-time equations, Journal of Applied Physics 85 (1999) 1471–1560.